DOI: 10.61782/fa.2025.0808

FORUM ACUSTICUM EURONOISE 2025

SPATIAL ANALYSIS OF AXIAL FAN PSYCHOACOUSTIC METRICS

Nejc Cerkovnik[1*] **Jurij Prezelj**[1]

[1] Laboratory for pumps, compressors and technical acoustics, University of Ljubljana, Slovenia

ABSTRACT

Efficient cooling solutions are crucial for high-performance computing environments, yet the noise generated by axial fans often detracts from user comfort and productivity. Traditional noise assessment metrics, such as sound pressure level (SPL) and A-weighted spectra is not sufficient in addressing the subjective sound quality and annoyance experienced. This study introduces a novel approach that utilise spatial analysis of the pressure field in front of the fan.

We scanned the pressure field across the surface at the inlet side of the axial fan. We calculated psychoacoustic metrics, namely loudness, sharpness, roughness, fluctuation strength, and tonality. Our visualizations reveal significant spatial variations in these metrics, indicating that certain areas at the fan inlet exhibit stronger psychoacoustic effects, which can be correlated with distinct flow regimes at the same area. These findings demonstrate that psychoacoustic metrics are not only reflective of sound quality but can also serve as indicators of the flow dynamics.

Our research shows the potential of using psychoacoustic metrics as tools for visualizing and optimizing flow regimes and therefore developing computer axial fans with more pleasant sounds.

Keywords: *axial fan, acoustics, psychoacoustics, aerodynamics, hot-wire*

1. INTRODUCTION

The noise emissions of small axial fans significantly affect acoustic environments, particularly in quiet spaces such as offices and medical facilities. These fans generate noise from multiple sources, including blade passing harmonics, turbulence-induced broadband noise, and vortex shedding. Excessive noise can reduce comfort and impair concentration, highlighting the importance of understanding noise generation mechanisms to improve design and efficiency.

One of the fundamental approaches to analysing noise sources in axial fans is flow visualization. By employing techniques such as smoke visualization, laser-induced fluorescence, or particle image velocimetry (PIV), researchers can gain insights into the unsteady aerodynamic phenomena responsible for noise emissions.

The velocity field in axial fans, particularly as mapped via hot-wire anemometry, is critical for understanding the aerodynamic performance and overall efficiency of fan systems. Numerous studies have employed hot-wire techniques to capture detailed flow characteristics, revealing significant insights into both steady and unsteady airflow dynamics. For instance, Jin et al. explored the three-dimensional flow characteristics of axial fans equipped with circumferential skewed blades, emphasizing the role of blade design on flow dynamics at off-design conditions [1]. Similarly, Šekularac and Janković performed an experimental and numerical analysis of flow fields in axial fans, utilizing HWA to measure key parameters such as mean flow velocities at the fan exit, turbulence intensity, and other flow characteristics [2-3].

Additionally, Caldas et al. highlighted the invasiveness of hot-wire probes and their effect on flow field measurements, emphasizing the meticulousness required in traverse measurements to minimize perturbations [4].

The application of hot-wire anemometry has proven particularly illuminating in turbulent flow studies. Matsushita et al. reviewed the use of hot-wire techniques to measure velocities in staggered tube bundles, highlighting the instrument's capacity to provide precise measurements in turbulent regimes [5]. This accuracy is crucial for understanding turbulence characteristics that can affect the efficiency and performance of axial fans.

[*] ***Corresponding author***: nejc.cerkovnik@fs.uni-lj.si.

Furthermore, Ocker et al. utilized a turbulence grid upstream of axial fans to generate inflow turbulence, assessing flow fields downstream using 3D hot-wire measurements to understand aerodynamic interactions [6].

The effects of inlet geometry and fan design have been investigated as well. Liu et al. examined how different inlet geometries influenced the flow performance and field around half-ducted propeller fans, leveraging hot-wire measurements to elucidate shifts in axial velocities as the opened area increased [7].

Moreover, examining the correlation between noise and velocity fluctuations has also been a focus. Hamakawa et al. explored the link between noise generation and velocity fluctuations from tip leakage flows in low-pressure axial fans [8]. They utilized hot-wire measurements to assess the periodic nature of velocity fluctuations near rotor tips, which is vital for noise management in fan design.

In particular, the concept of pseudosound is used to differentiate between acoustic and hydrodynamic pressure fluctuations in turbulent flows. Pseudosound, which represents non-acoustic pressure variations associated with vortical structures, plays a significant role in characterizing flow-induced noise sources. By distinguishing between true acoustic waves and convective pressure fluctuations, researchers can better understand and control the noise mechanisms in small axial fans.

In addition to flow visualization and the study of axial fan acoustics extends into the domain of psychoacoustics. The human perception of noise is not solely determined by physical sound pressure levels but also by its spectral composition, temporal structure, and subjective annoyance. Psychoacoustic metrics, such as loudness, sharpness, roughness, and fluctuation strength, provide valuable tools for assessing the impact of fan noise on human listeners. By integrating psychoacoustic evaluation with aerodynamic and acoustic analysis, a more comprehensive understanding of axial fan noise can be achieved, leading to the development of quieter and more perceptually optimized designs [9-?].

Despite extensive research on axial fan acoustics, a critical limitation remains: previous studies evaluate psychoacoustic metrics using a single value for each fan, disregarding spatial variations. This study aims to address this gap by demonstrating that psychoacoustic metrics can be spatially visualized across the inlet surface of an axial fan. By mapping psychoacoustic effects in relation to airflow structures, we propose a novel method for identifying and mitigating the most annoying noise components. This approach has the potential to improve fan designs by linking psychoacoustic perception directly to aerodynamic phenomena.

2. METHODOLOGY

2.1. Axial fan used in this study

All measurements were carried out on the same low-pressure axial fan with housing dimensions of 120x120 mm. Its thickness was 25 mm. Further dimensions and operating parameters of the fan are shown in Table 1 and the fan is also shown in Figure XX. Its speed was kept constant using a controller and special software. In order to maintain its position in the room, which was crucial when using traversing system, we installed the fan in a rigid wall.

Table 1: Dimensions and operational parameter of the axial fan used in study.

Rotational speed- n [RPM]	2000
Volumetric flow rate at FD condition - Q [m^3/h]	118
Number of blades – N_b [/]	7
Hub diameter - D_h [mm]	45
Blade tip diameter - D_t [mm]	115

2.1 Traversing system

In order to perform consistent measurements at the same location, we built a 3-axis traversing system. Special software was written in the LabView programming environment to traverse the selected point grid and simultaneously perform the measurement at each point.

2.2 Pressure measurements

For the first part of the measurements, where the pressure field was of interest, we mounted the 1/2" Superlux EMC888B microphone on traversing system and carried out the measurement at 361 points at a distance of 20 mm in front of the axial fan. The sampling area extended 30 mm from the edges of the fan housing, i.e. a square with the dimensions 180x180 mm, in order to also sample areas outside the fan rotor. The microphone signal was recorded with the Motu Stage B-1 at a sampling frequency of 48 kHz. The entire measurement system was housed in an anechoic chamber in the LEDSTA laboratory.

2.3 Velocity measurement

The second part of the measurements consisted of measuring the velocity field in front of the axial fan. For this purpose, we mounted a hot-wire probe on the traverse system. We used a calibrated Dantec 55P11 1D hot wire anemometer with a combination of MiniCTA and Data Translation's DT9837C A/D converter to perform three rounds of measurements, rotating the probe to measure the flow in three different axes – x, y, z, which correspond to the global axes also used by the traverse system.
The signals recorded with the anemometer were converted into velocities using King`s law and the constants determined during calibration. The velocity fluctuation $w(t)$ was calculated using equation XX.

$$w(t) = u(t) - U_{mean} \quad (1)$$

Where u(t) stands for measured instantaneous velocity and U_{mean} time-averaged velocity.

2.4 Psychoacoustic metrics

The psychoacoustic metrics were calculated from the recorded signals of velocity fluctuations and signals from microphone using the sound quality algorithms implemented in the NI LabVIEW Sound and Vibration (SV) Toolkit. The mentioned toolkit consists of the following algorithms, which were also used in our study: time-varying loudness, Aures roughness, Aures sharpness, Aures tonality and fluctuation strength.
Algorithm for time varying loudness measures 1/3 octave spectrum using exponential averaging with a 2 ms time constant, combines the fractional-octave bands into critical bands, and applies temporal and spectral masking. This algorithm then returns the result as the specific loudness versus critical band rate, integrates the specific loudness, and applies temporal post-masking filters to measure the time-varying loudness. This algorithm calculates the time-varying loudness in compliance with DIN 45631/A.
Roughness correlates to how noticeable or annoying a sound is as heard by the human ear. More specifically, roughness is a hearing sensation related to loudness modulations at frequencies too high to discern separately, such as modulation frequencies greater than 30 Hz. The roughness algorithm measures the energy in 24 barks, computes and filters the envelope of the signal in each band, measures the amplitude modulation of each envelope, and then weights the level in each band using both the modulation index of that band and a frequency-dependent weighting function. The algorithm returns the result as the roughness spectrum versus critical band rate and then integrates the roughness spectrum to measure the roughness.
Sharpness corresponds to the sensation of a sharp, painful, high-frequency sound and is the comparison of the amount of high frequency energy to the total energy. The sharpness algorithm computes sharpness from the sound pressure signal waveform, the 1/3-octave band spectrum calculated over the frequency range 25 Hz to 12.5 kHz, or the specific loudness. This algorithm normalizes the specific loudness spectrum by the total loudness and weights the spectrum according to frequency. The algorithm returns the frequency-weighted result as the specific sharpness versus critical band rate and then integrates the specific sharpness to measure the sharpness. Higher frequency components in the signal generally result in higher sharpness measurements.
Tonality is used to determine whether a sound consists mainly of tonal components or broadband noise. The algorithm measures the relative strength of the tones in a signal compared to the overall signal. For each time block, this algorithm first varies the frequency resolution according to the frequency selectivity of human hearing, searches the spectrum for likely tones, and then compares the loudness of the tones to the loudness of the sound.
Fluctuation strength is a hearing sensation related to loudness modulations at low frequencies that are discernible individually. Fluctuation strength uses a similar method to "roughness versus time" analysis except that it focuses specifically on signal variations with very low modulation frequencies. Fluctuation strength measures the energy in 47 overlapping barks, computes and filters the envelope of the signal in each band, measures the amplitude modulation of each envelope, and weights the level in each band using a frequency-dependent weighting function. The algorithm returns the result as the fluctuation strength spectrum versus critical band rate and then integrates the fluctuation strength spectrum to measure the fluctuation strength. The algorithm examines modulations between 0 to 30 Hz, with special emphasis on those near 4 Hz

2.5 Correlation computation

To evaluate the correlation between the pressure and velocity fields, we plotted the values of L_{eq} and the psychoacoustic metric on the heat map, assigning this value to the coordinate where the original signal was measured. To find a linear correlation between these two fields of the selected variables, the Pearson correlation and Cosine

similarity coefficient was calculated. All data was post-processed using programs written in Python.

3. RESULTS AND DISCUSSION

The frequency spectra of pressure and velocity fluctuation can be seen in Fig. 1. Signals were sampled at the position (50,0) mm. The origin of the coordinate system is located in the centre of the hub. This position corresponds to the area of the blade tip.

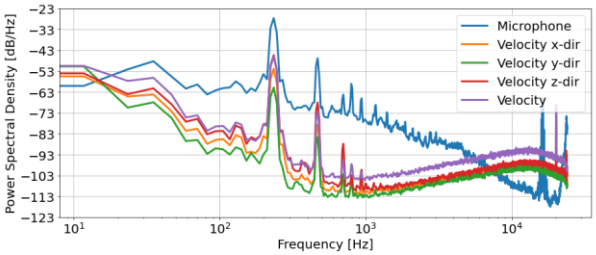

Figure 1: Power spectral density of pressure and velocity measured 20 mm in front of the axial fan at position (50,0) mm.

It can be seen that the tonal peaks of the spectra corresponding to the blade passage frequency (BPF) and its multiples match well with the pressure and velocity fluctuations, confirming that the hot-wire anemometer can detect the particle motion associated with acoustic radiation.

The heatmap obtained for the pressure field are shown in Fig. 2 and for the velocity field in Fig. 3. The spatially distributed values of the individual metrics are shown in the same way for pressure and velocity signals. In all images, these values are normalized so that they vary between 0 and 1. The colours of the heatmap correspond to this normalization, so that the red colour represents values close to 1 and the blue colour close to 0. We opted for this type of representation because only the spatial position of the individual metrics is important, not their magnitude. The black rectangle represents the outer edge of the housing of the axial fan, the large circle the inner edge of the housing and the smaller circle the edge of the hub of the fan.

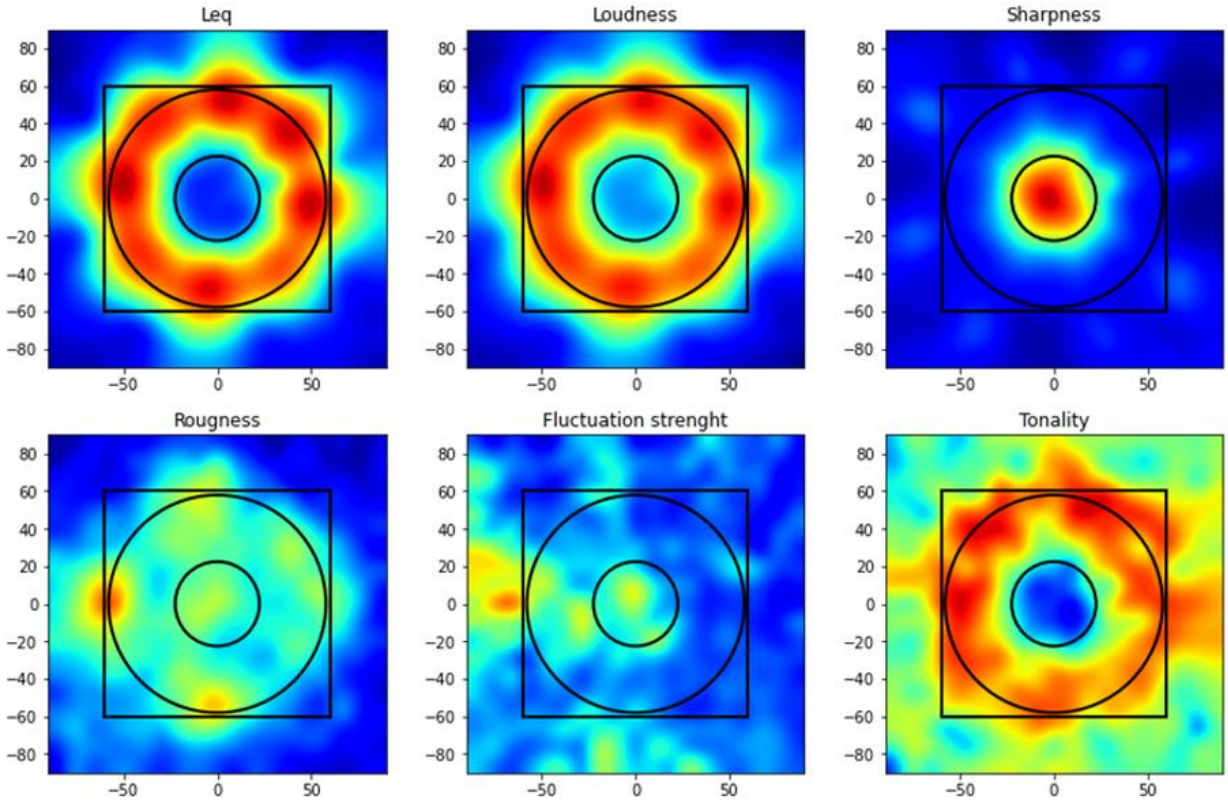

Figure 2: Normalized values of psychoacoustic metrics calculated from pressure signal.

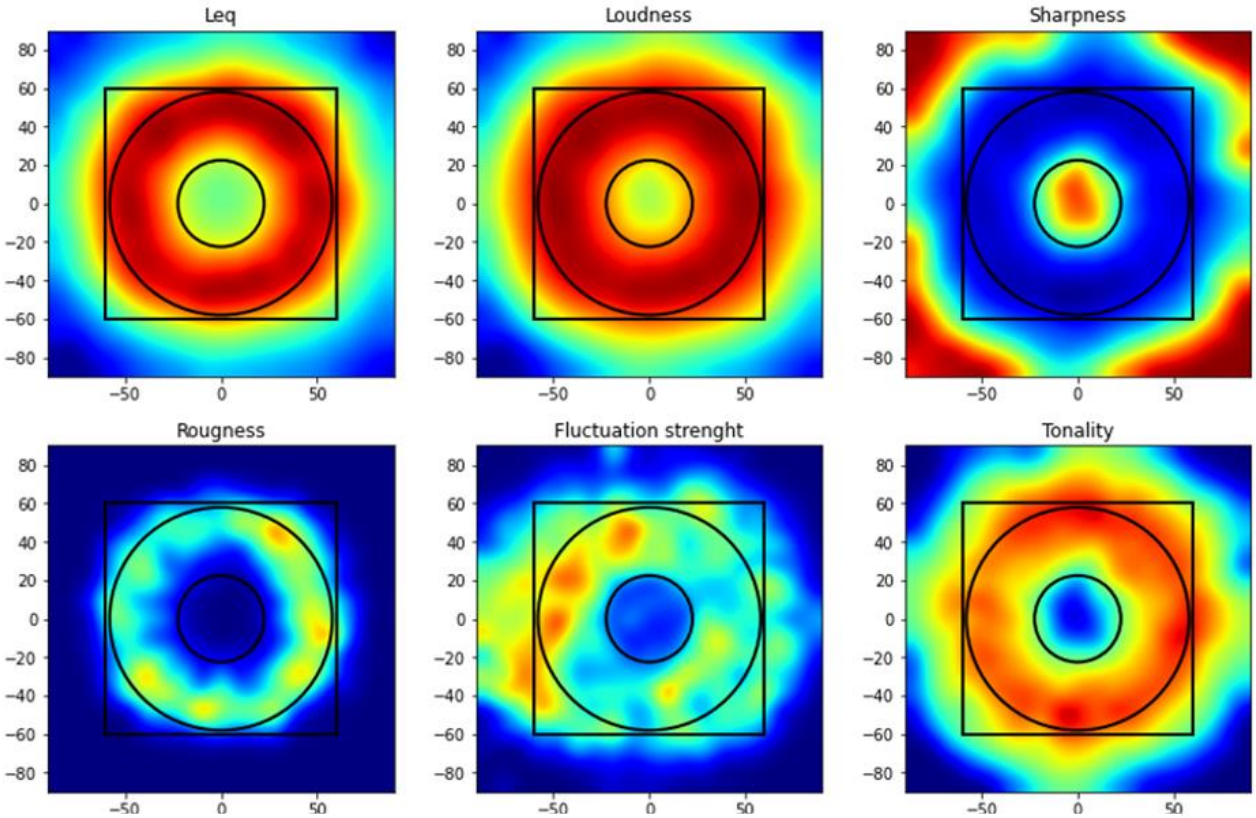

Figure 3: Normalized values of psychoacoustic metrics calculated from velocity fluctuations.

L_{eq} is shown first. Here a comment must be added to the L_{eq} representation of the velocity fluctuation, which was calculated in identical way as the pressure signal, using the same reference value (2e-5 m/h). It can be seen that similar areas are covered with red colour, especially the area between the half length of the blades, which extends beyond the blade tip. As in the case of velocity, this area has a pronounced circular shape, and we can observe that in the case of the pressure signal, this ring consists of 8 circles. L_{eq} corresponds to the level of the entire frequency spectrum of the signal but can also indicate the location of the dominant component.

A similar pattern emerges with the first psychoacoustic metric, namely loudness. We can see that the area where this metric is intense increases in both directions of the hub and more outside the blade tip region compared to the L_{eq}. For loudness, the very low and very high frequency components are weighted less, so most of the noise in the audible spectra is generated aerodynamically in the region between the hub, blade tip and edge of housing.

Sharpness has a completely different shape than the first two metrics. Sharpness corresponds to the amount of high-frequency content in the signal. Interestingly, the patterns of velocity and pressure signal do not overlap as well as with L_{eq} and Loudness. A similar area is just the region of the hub, and we can see that in the case of the velocity signal, the sharpness pattern is extended into the area outside the strict axial fan area. We can refer to this area as the area where the SNR ratio of the velocity signal was the lowest, because no mean velocity was measured here or it was very low, which means that the air is not moving in this area. On the other hand, the pressure field in the hub area can confirm the high frequency content emanating from this location, as the motor is known to be the source for this area of the audible spectrum.

Roughness is the measure of loudness modulation above 30 Hz. Its spatial distribution is very different for velocity and pressure data. In the case of velocity, the roughness is higher in the area of the blade tips. In the case of the pressure signal, the roughness is also high in the hub area. In the location of the blade tips, the donut shape is not continuous but radiates from 3 different points on the black circle and the right point, which is slightly fuzzier.

The patterns cannot be visually correlated for the fluctuation strength, the measure for the loudness modulations below 30 Hz, either. Again, a clearer pattern emerges for the velocity signal, where higher values of fluctuation strength are limited to the area outside the hub and are clearly associated with locations where airflow is present. In the case of the pressure signal, the pattern is not even symmetrical. We must add here that the amplitude range of the fluctuation strength is very small and therefore does not represent a distinct sound component in a typical axial fan.

Tonality, on the other hand, shows a spatial correlation between the two fields. Here, too, the area of higher tonality amplitudes lies outside the hub and spreads out into space beyond the area of the axial fan housing. In both cases, the donut shape is not round as in the case of loudness, but has peaks at some points around the circumference. The source of the tonality are blades passing by the microphone and the alternation between the pressure and suction sides of them. When the microphone is close to the blades, the passage of the blades is clearly visible in the recorded signal. It propagates from this area, but is influenced by coherent sources from elsewhere in the fan. Therefore, it is attenuated in some places and amplified in others.

The Person correlation coefficient and cosine similarity coefficient for each of the metrics is presented in Table 2. We can see that correlation is high for L_{eq} and loudness. We can say that there is also a correlation between field at computed tonality and roughness, but hardly saying this for fluctuation strength and sharpness. We must emphasize that in the strict region of axial fan Sharpness has similar pattern in both fields, but both correlation coefficients show week correlation due to the misaligned region outside of the fan.

Table 2: Pearson correlation and Cosine similarity coefficient for each metric calculated between pressure and velocity signal.

	L_{eq}	Loud.	Sharp.	Rough.	Fluc. Str.	Tonality
Pear.	0.93	0.96	0.06	0.55	0.18	0.64
Cos.s.	0.97	0.98	0.56	0.71	0.75	0.93

We also calculated SPL in 1/3 octave frequency bands for pressure and velocity signals in each scanning point and again proceed with computation of Cosine similarity and Pearson coefficients. Results can be seen in Fig.4. We can see that cosine similarity coefficient is very high through all of the frequency bands, indicating strong vector alignment between two fields. The Pearson correlation coefficient also shows a generally high correlation (above 0.8 in most of the spectrum), but with more noticeable fluctuations. Significant drop is observed at higher frequencies (10^4 Hz).

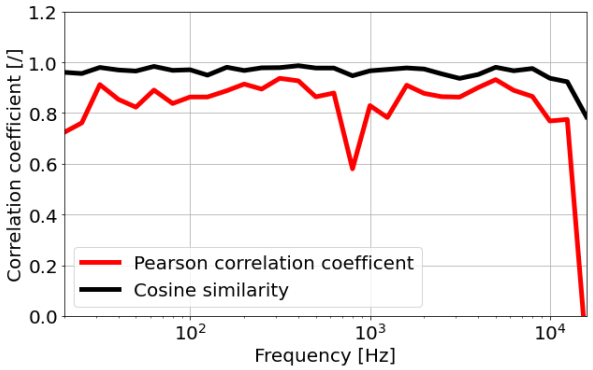

Figure 4: Pearson correlation and Cosine similarity coefficient for each 1/3 octave band calculated between pressure and velocity signal.

4. CONCLUSION

This study investigated the correlation between psychoacoustic metrics derived from pressure and velocity fields in front of a low-pressure axial fan. By employing a 3-axis traversing system, we systematically measured the pressure fluctuations using a microphone and the velocity field using a hot-wire anemometer. The data was analysed using psychoacoustic algorithms to evaluate loudness, sharpness, roughness, fluctuation strength, and tonality.

The results demonstrate a strong spatial correlation between the pressure and velocity fields, particularly in the L_{eq} and loudness distributions, which highlight the dominant noise-generating regions near the blade tips and housing edges. While sharpness and roughness showed different spatial patterns for pressure and velocity signals, tonality exhibited a clear correlation, reinforcing the role of blade passage effects in tonal noise generation.

Furthermore, correlation analysis across the third-octave frequency spectrum revealed that while the cosine similarity remained high, the Pearson correlation coefficient fluctuated, particularly at higher frequencies (~10^4 Hz). This suggests that acoustic radiation and airflow dynamics become increasingly decoupled at higher frequencies, possibly due to turbulence effects and differences in how pressure and velocity fluctuations propagate.

These findings provide valuable insights into aeroacoustics noise generation mechanisms in axial fans. The strong correlation between velocity and pressure-based

psychoacoustic metrics suggests that hot-wire anemometry could serve as a complementary tool for acoustic analysis, particularly in environments where microphone-based measurements are challenging. Future studies could extend this approach to different fan designs, operating conditions, and flow regimes to further refine our understanding of fan noise generation and perception.

5. ACKNOWLEDGMENTS

The authors acknowledge the financial support from the Slovenian Research Agency (research core funding No. P2-0401).

6. REFERENCES

[1] G. Jin, H. Quyang and Z. Du: "*An experimental study of sweep effect on 3d flow downstream of axial fans at off-design conditions*", App. Mechanics and Materials, vol. 281, pp. 335-342, 2013

[2] M. Šekularac: "*Experimental determination of tunnel ventilation axial ducted fan performance*", Thermal Science, vol. 20(1), pp. 209-221, 2016.

[3] M. Šekularac and N. Janković: "*Experimental and numerical analysis of flow field and ventilation performance in a traffic tunnel ventilated by axial fans*", Theoretical and Applied Mechanics, vol. 45(2), pp. 151-165, 2018

[4] L. Caldas, C. Kissner and R. Meyer: "*Comparison of techniques for the estimation of flow parameters of fan inflow turbulence from noisy hot-wire data*", Fluids, vol. 6, 2021.

[5] Y. Matsushita, Y. Hagiya and H. Aoki: "*Experimental and numerical investigations of turbulent flow in a staggered tube bundle*", Isij International, vol. 60(6), 2021.

[6] C. Ocker, F. Czwielong and S. Becker: "*Aerodynamic and aeroacoustic properties of axial fan blades with slitted leading edges*", Acta Acustica, vol. 6, pp. 48, 2022.

[7] P. Liu, N. Shiomi and T. Setoguchi: "*Effect of inlet geometry on fan performance and flow field in a half-ducted propeller fan*". Int. Jour. of Rotating Machinery, vol. 2012, pp. 1-9, 2012.

[8] H. Hamakawa, M. Shiotsuki, T. Adachi and E. Kurihara: "*Correlation between aerodynamic noise and velocity fluctuation of tip leakage flow of axial flow fan*". Open Journal of Fluid Dynamics, vol. 2 (4), pp. 228-234, 2012.

[9] T. Novaković, L. Čurović, M. Hočevar and J. Prezelj: "*Impact of geometric modifications of small axial fans on psychoacoustic metrics*", App. Acoustics, vol. 218, 2024.

[10] A. Cattanei, M. Zecchin and A. Lazari: "*Effect of the uneven blade spacing on the noise annoyance of axial-flow fans and side channel blowers*", App Acoustics vol. 117, 2021.